TABLE 1 Growth of Ba/F3 cells after infection*

Ba/F3 cells infected by	Medium supplemented with IL-3	Epo	None
None	+	−	−
SFFV	+	−	−
SF-ER	+	+	−
SFFV + SF-ER	+	+	+

* About 5×10^5 Ba/F3 cells were infected with SFFV, SF-ER, or both. After infection, the cells were kept for 24 h in IL-3 (10% WEHI-3 supernatant) before switching to either erythropoietin (Epo; 0.5 units per ml) or regular medium without any added growth factors. Positives (+) represent cultures (of 5×10^5 cells) with rapidly growing cells that became established within one week of infection. Negatives (−) represent cultures with no viable cells left within 3-4 days after infection and no cell growth even after up to one month of incubation.

Friend erythroleukaemia cell lines tested continue to express gp55 when maintained in culture while expression of other virus-encoded proteins may cease[19], interaction between gp55 and Epo-R may still be necessary to maintain the malignant status of late-stage leukaemic cells; our results indicate that this protein interaction does persist in these cells. It is the intracellular form of gp55, and not the larger form localized on the cell surface, that is bound to Epo-R. Therefore, the interaction between the two proteins probably occurs in the endoplasmic reticulum. Because the plasma membrane form constitutes only ~5% of the total SFFV glycoprotein[6], its possible binding to Epo-R would be difficult to detect.

The ability of gp55 to stimulate cell proliferation by binding to the erythropoietin receptor represents a novel mechanism by which viruses can override normal growth-regulating functions. It will be of interest to see whether other viruses use similar mechanisms to cause proliferation of specific cell types. For instance, the envelope glycoproteins encoded by several oncogenic mink cell focus-forming viruses (MCFs) are structurally related to SFFV gp55 (refs 20, 21). Because the amino-acid sequence of Epo-R is similar to that of the β-subunit of the IL-2 receptor[22], it is possible that the MCF envelope glycoprotein interacts with the IL-2 receptor or another member of this group of growth factor receptors, thereby causing MCF-induced T-cell leukaemia. □

Received 16 October; accepted 19 December 1989.

1. Bestwick, R., Hankins, D. & Kabat, D. *J. Virol.* **56,** 660-664 (1985).
2. Friend, C. *J. exp. Med.* **105,** 307-318 (1957)
3. Hankins, D., Kost, T., Koury, M. & Krantz, S. *Nature* **276,** 506-508 (1978).
4. Hankins, D. & Troxler, D. *Cell* **22,** 693-699 (1980).
5. Wolff, L. & Ruscetti S. *Science* **228,** 1549-1552 (1985).
6. Dresler, S., Ruta, M., Murray, M. & Kabat, D. *J. Virol.* **30,** 564-575 (1979).
7. Ruta, M., Clarke, S., Boswell, B. & Kabat, D. *J. biol. Chem.* **257,** 126-134 (1982).
8. Ruscetti, S. & Wolff L. *J. Virol.* **56,** 717-722 (1985).
9. Li, J.-P., Bestwick, R., Machida, C. & Kabat, D. *J. Virol.* **57,** 534-538 (1986).
10. Linemeyer, D., Menke, J., Ruscetti, S., Evans, L. & Scolnick, E. *J. Virol.* **43,** 223-233 (1982).
11. Ruta, M., Bestwick, R., Machida, C. & Kabat, D. *Proc. natn. Acad. Sci. U.S.A.* **80,** 4704-4708 (1983).
12. Linemeyer, D., Ruscetti, S., Scolnick, E., Evans, L. & Duesberg, P. *Proc. natn. Acad. Sci. U.S.A.* **78,** 1401-1405 (1981).
13. Li, J.-P., Bestwick, R., Spiro, C. & Kabat, D. *J. Virol.* **61,** 2782-2792 (1987).
14. Danos, O. & Mulligan, R. *Proc. natn. Acad. Sci. U.S.A.* **85,** 6460-6464 (1988).
15. D'Andrea, A., Lodish, H. & Wong, G. *Cell* **57,** 277-285 (1989).
16. Mathey-Prevot, B., Nabel, G., Palacios, R. & Baltimore, D. *Molec. cell. Biol.* **6,** 4133-4135 (1986).
17. Mirand, E. *Science* **156,** 832-833 (1967).
18. Moreau-Gachelin, F., Tavitian, A. & Tambourin, P. *Nature* **331,** 277-280 (1988).
19. Anand, R., Lilly, F. & Ruscetti, S. *J. Virol.* **37,** 654-660 (1981).
20. Ruscetti, S., Linemeyer, D., Feild, J., Troxler, D. & Scolnick, E. *J. Virol.* **30,** 787-798 (1979).
21. Adachi, A. *et al. J. Virol.* **50,** 813-821 (1984).
22. D'Andrea, A., Fasman, G. & Lodish, H. *Cell* **58,** 1023-1024 (1989).
23. Bestwick, R., Kozak, S. & Kabat, D. *Proc. natn. Acad. Sci. U.S.A.* **85,** 5404-5408 (1988).

ACKNOWLEDGEMENTS. We thank Dr D. Kabat for providing the pSFF vector. We are grateful to Drs D. Kabat, H. Varmus, D. Hankins, S. Ruscetti and G. Fasman for discussion. This work was supported by an NIH Physician Scientist Award to A.D.D.'A., and by NIH grants to H.F.L. and D.B.

Ion channels in the nuclear envelope

Michele Mazzanti, Louis J. DeFelice, Jacques Cohen* & Henry Malter*

Department of Anatomy and Cell Biology, Emory University School of Medicine, Atlanta, Georgia 30322, USA

CELL nuclei are capable of partitioning a wide variety of molecules from the cytosol, including macromolecules such as proteins[1-11] and RNA[12-14], and smaller peptides[9,14-16], amino acids[17], sugars[18,19] and Na^+ and K^+ ions[20,21], all of which can be accumulated in or excluded from the nuclear domain. There are two mechanisms behind this compartmentalization: selective retention of freely diffusible molecules, and selective entry through the nuclear envelope. It is generally accepted that the nuclear envelope restricts only the larger molecules[22-24]. Here we apply the patch-clamp technique to isolated murine pronuclei[25] and show that the nuclear envelope contains K^+-selective channels which have multiple conductance states, the maximal conductance being 200 pS. These channels, which contribute to the nuclear membrane potential[26], may be important in balancing the charge carried by the movement of macromolecules in and out of the nucleus.

Nuclear envelopes contain pores for the selection of macromolecules, but these pores are considered to be too large to act as barriers against ions[22-24]. Nevertheless, electrical potential across nuclear envelopes and segregation of ions in the nucleoplasm have been reported[21,26,27], indicating that there could be ion-selective channels in the nuclear membrane. We have repeated the nuclear resting-potential measurements *in situ* in murine zygotes. Using an enucleation procedure[25] (Fig. 1), we compare these results with nuclear potentials and patch-clamp recordings in cell-free nuclei.

The average potential between the nucleoplasm and the cytoplasm, from the protocol shown in Fig. 2*a*, is -10.75 ± 1.25 mV ($n = 4$). After placing the zygote in a solution of 120 mM K^+/0 mM Na^+ (*b*) to null its resting voltage, the nuclear potential becomes -9.87 ± 0.85 mV ($n = 4$). A cell-free nucleus in the same solution (*c*) has a potential of -9.5 ± 2.08 mV ($n = 4$), and in a 60 mM K^+/60 mM Na^+ solution (*d*) the potential is -23.5 ± 4.2 mV ($n = 4$). The hyperpolarization that takes place following this change in the composition of the external solution indicates that a K^+ selective mechanism could be operating in the nuclear envelope.

To investigate the possibility that this mechanism involves ion-selective channels, we formed nuclear-attached patches on extracted pronuclei. Figure 3*a* shows patch currents at pipette voltages (V_p) equal to +20, −20, +30 and −30 mV. Examples of the single-channel records at $V_p = -10$ mV are shown in *d* on a faster timescale. To obtain the absolute voltage, we used $V = (V_{rest} - V_p)$, where V_{rest} is the nuclear potential from Fig. 2*c*. From the current-voltage ($i(V)$) curves in Fig. 3*c*, which are obtained by plotting the currents at the peaks of the amplitude histograms in Fig. 3*b*, the conductances of the channel are 200 and 55 pS, and its reversal potential is −9 mV, which is roughly equal to the nuclear resting potential in the same solution.

Figure 4 summarizes five experiments with 60 mM K^+/60 mM Na^+ in the pipette and 120 mM K^+/0 mM Na^+ in the bath. The dominate conductance is now 75 pS, and the reversal potential ranges between −21 mV and −15 mV. We assume that this channel corresponds to the 200 pS conductance in Fig. 3, because longer steps fail to show higher conductances (inset in Fig. 4). In addition, channel activity at $V_p = 0$ mV implies there

* Present address: Center for Reproductive Medicine and Infertility, Department of Gynecology and Obstetrics, Cornell University Medical College, 505 East 70th Street, New York, New York 10021, USA.

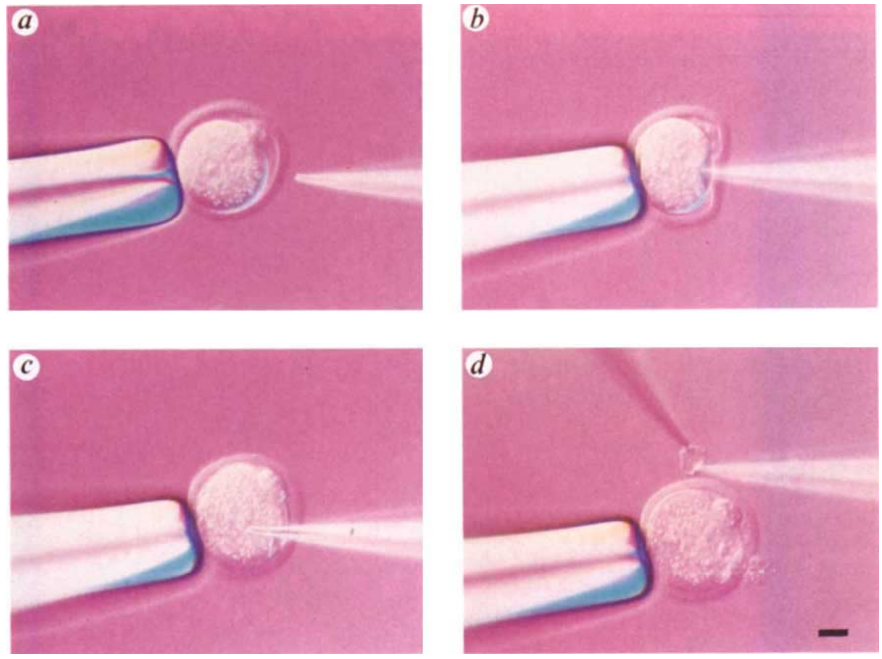

FIG. 1 A summary of the procedure we used for the transfer of viable pronuclei, adapted to intracellular microelectrode and patch-clamp recording. The scale bar in *d* indicates 20 μm. Female B6D2 F_1 mice were superovulated using 5 IU of pregnant mare serum gonadotropin (Organon, Holland), which was followed in 48 h by 5 IU human choriogonadotropin (Sigma) and individual mating with B6D2 F_1 males. Zygotes were collected ~12 h after mating. Cumulus cells were removed from the zygotes by incubation in a 1% hyaluronidase solution for several minutes. After transferring the zygote to the bath solution (in mM: 120 KCl, 2 $MgCl_2$, 1.1 EGTA, 0.1 $CaCl_2$, 5 glucose, 10 HEPES, pH 7.4), which is a cytoplasmic-like solution used in the intracellular electrode to perform whole-cell experiments on mouse oocytes, we extracted one of the pronuclei using micromanipulation[25]. The sequence of steps from holding the zygote by the zona with light suction (*a*), entering the zygote with a smaller suction pipette (*b*), attaching it to the pronucleus (*c*), and extracting and holding the pronucleus for patch clamping (*d*), takes less than 10 min. In *d*, the third pipette on the top is a patch electrode placed on the nuclear envelope surface. We made no attempt to distinguish sperm and oocyte pronuclei in either the resting potential or the single-channel measurements. To measure intracellular and intranuclear membrane potentials, we used an Axoclamp amplifier and glass microelectrodes (70 to 90 megohm, filled with 3 M KCl), which we balanced off with the bridge circuit. The patch electrodes were pulled from hard borosilicate glass (Corning 7052) on a Sachs-Flaming P-84 puller (Sutter Instruments). The pipettes were coated with Sylgard (Dow Corning) and fire-polished to an external tip diameter of ~1–2 μm. These electrodes had resistances of 4–10 megohms. The estimated surface area of the patch formed with these electrodes is between 5 and 6 μm^2. Using a List EP-7 current-to-voltage converter, we applied standard cell-attached patch techniques to obtain 1–10 gigohm seal, nucleus-attached patches from pronuclei. In the single-channel experiments, the pronucleus was bathed in standard 120 mM K^+ cytoplasmic-like solution; the patch pipette contained either this same solution or a 60 mM K^+/60 mM Na^+ solution. We performed the experiments immediately after extracting the pronucleus, pressing the electrodes against areas of the nuclear membrane that appeared to be clear of cytoplasmic material (*d*).

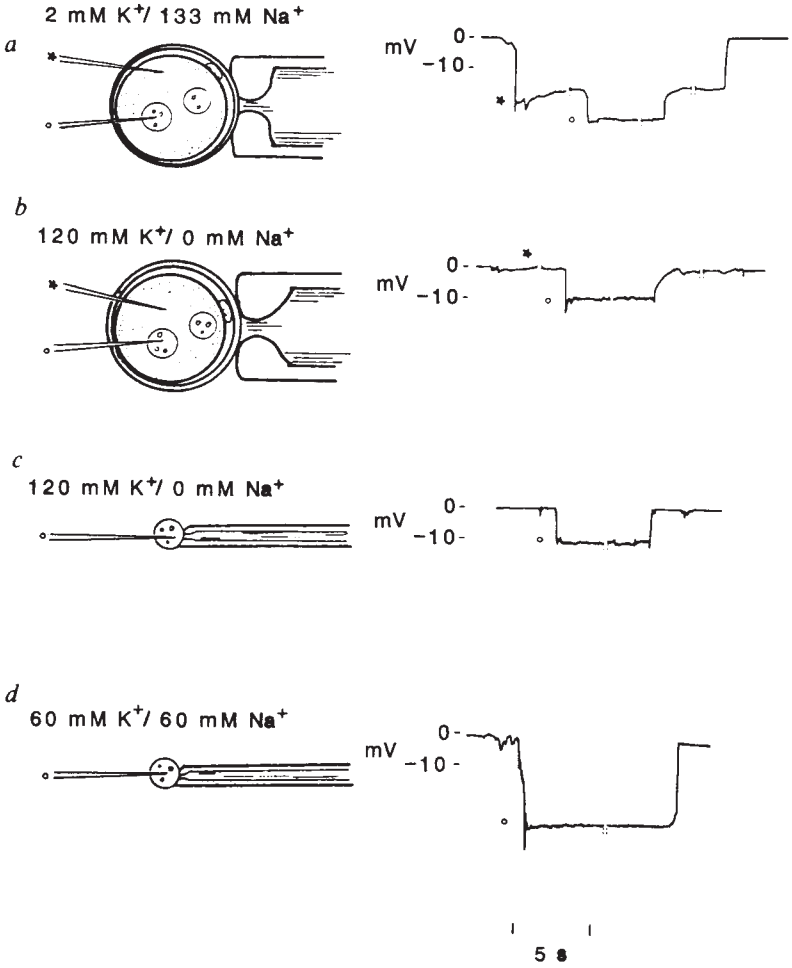

FIG. 2 We performed four types of resting potential experiments. *a*, With the zygote bathed in an extracellular-like solution (in mM: 133 NaCl, 2 KCl, 1.5 $CaCl_2$, 0.5 $MgCl_2$, 10 HEPES, 5 glucose, pH 7.4), we set the electrode tip potential to zero. We then inserted he microelectrode into the cytoplasm to record the cell membrane potential (*). Under visual control, we then drove the microelectrode into the pronucleus to record the nuclear membrane potential with respect to the cytoplasm (circles). In *b*, we followed this same procedure, now bathing the zygotes in the cytoplasmic-like solution used in the pronuclear extraction (see Fig. 1) to abolish the cell membrane potential. Here we set the electrode tip potential to zero in the cytoplasmic-like solution. In *c*, we directly measured the nuclear membrane potential by extracting the pronucleus and bathing it in the cytoplasmic-like solution (see Fig. 1) and finally, in *d*, we repeated the direct measurement on the pronucleus after replacing the 120 mM K^+ in the cytoplasmic-like solution with 60 mM K^+/60 mM Na^+. During measurement of resting potentials, we estimated resistances by rebalancing the bridge after entering the nucleus, which indicated that nuclear resistances are less 1 megohm. We discarded records unless the potentials reversed upon withdrawal. All experiments were at room temperature (26–28 °C).

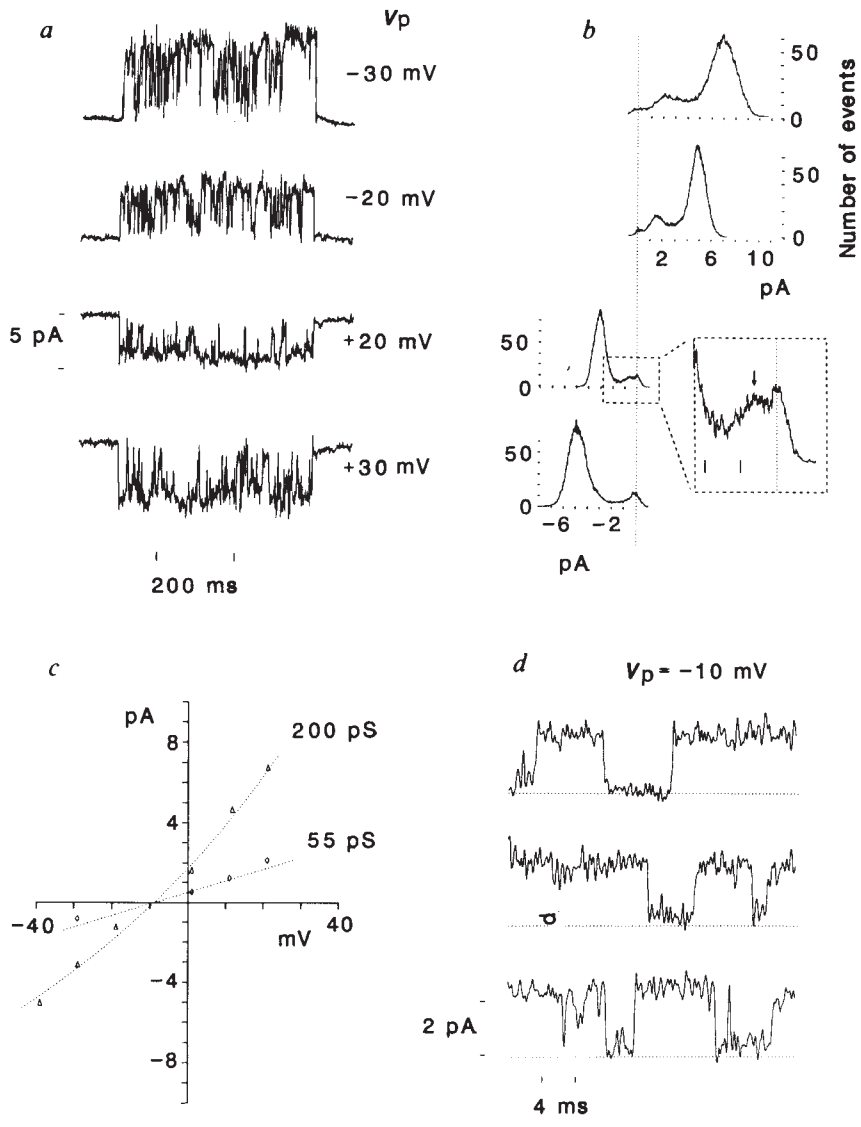

FIG. 3 Single-channel measurements from the nuclear envelope. *a*, Examples of current traces elicited by: +20 and −20 mV, +30 and −30 mV steps. Seal resistances ranged from 1 to 10 gigohms. All traces are leak-subtracted. *b*, Examples of amplitude histograms derived from six concatenated current traces; each of the six traces is from the same experiment and is similar to the example shown to the left of each histogram. Thus a total of 3 s of data went into each histogram at each voltage. We assumed the first peak on each histogram (the dotted vertical line) to represent zero current. The second peak, which is more prominent in the outward direction, is barely visible at $V_p = +20$ (inset) and is unresolved at $V_p = +30$. In *c*, we plot the $i(V)$ relation, using the average nuclear membrane potential, −9.5 mV from protocol *c* (Fig. 2) to find the absolute membrane potential. The open triangles are the currents at the centre of the larger peaks, and the dotted line is a non-linear, least-squares fit to these points. The conductance is ~200 pS. Another smaller peak, more evident when the channel conducts outward current, is also plotted (open diamonds). This second smaller peak, with conductance of ~55 pS, is evident in the top two histograms, but is generally absent for the inward currents. The blow-up inset for the histogram at $V_p = +20$ mV shows data from a hyperpolarizing potential in which the smaller peak (arrow) is barely visible; the current read from the inset is the only inward current on 55 pS line. In 55 separate experiments, the 200 pS channel appeared in ~10% of the patches; the other patches contained either no channels (10%) or smaller conductance channels (80%), matching the lower conductances that appear when the 200 pS opening was present. Thus, channels are present in nearly every patch, but they are rarely in the highest conductance state. In all single-channel experiments the high-frequency cutoff was set at 1,000 Hz before analysis.

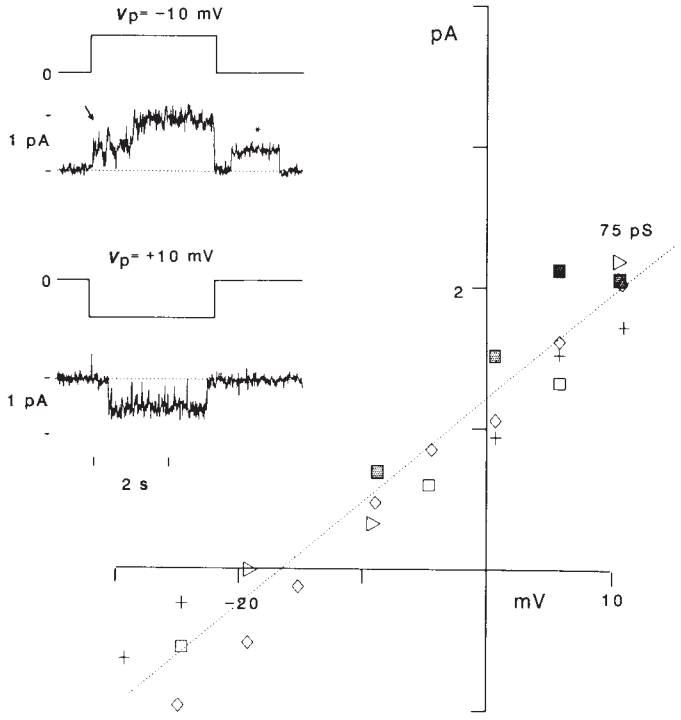

FIG. 4 To investigate channel selectivity, we filled the patch pipette with a 60 mM K^+/60 mM Na^+ solution while bathing the nucleus in the 120 mM K^+ solution (Figs 1 and 2). The points on the $i(V)$ plot are from five separate nuclei. The current levels were derived from lines drawn through the centres of the largest openings at the different voltages. The voltages are calculated from the equation, $V = (-9.5 - V_p)$. In the upper left quadrant we show examples of two voltage steps and the accompanying current traces at $V_p = -10$ mV and +10 mV. The arrow in the top trace indicates conductance levels lower than we used in the $i(V)$ plot. An example of an opening at $V_p = 0$ (*) also appears in the top current trace, something we never see with 120 mM K^+ in the pipette. The points at $V_p = +10$, 0 and −10 mV are plotted as diamonds. The cutoff frequency is 1,000 Hz.

is a driving force in 60 mM K^+/60 mM Na^+ that we never see in 120 mM K^+/0 mM Na^+.

The evidence for a K^+-selective pathway in the nuclear membrane can be summarized as follows: (1) decreasing the K^+ in the bath of the entire nucleus from 120 mM to 60 mM shifts the nuclear resting potential from −9.5 to −23.5 mV; (2) decreasing the K^+ in the patch from 120 mM to 60 mM shifts the reversal potential of channels in the patch from −9.5 to between −21 and −15 mV; (3) decreasing the K^+ in the patch from 120 to 60 mM also lowers the conductance of the channel from 200 to 75 pS. Assuming that K^+ is 20% more concentrated in the nucleus than in the cytoplasm[20], a K^+-selective membrane would generate −10 mV in 120 mM K^+ and −26 mV in 60 mM K^+, which are roughly equal to the nuclear potentials in these same solutions. Although −10 mV is near the reversal potential of the nuclear channel in 120 mM K^+, −26 mV is significantly higher than the reversal potential in 60 mM K^+, from which we infer that the channels are not exclusively responsible for the nuclear potential.

The nuclear channel is similar in some respects to the K^+-selective pore in the sarcoplasmic reticulum[28,29], which is continuous with the outer membrane of the nuclear envelope, but the sarcoplasmic reticulum channel in neutral bilayers has a conductance of ~100 pS in symmetric 120 mM KCl and 50 pS in 120 mM NaCl; also its conductance is linear from −100 mV to 70 mV. Despite these differences, our experimental conditions are too dissimilar to exclude the possibility that the channel we observe in cell-free nuclei is a sarcoplasmic reticulum-like pore.

Electron micrographs of our preparation indicate 3.3 pores per μm^2, or 4,000 per nucleus. If the channels are the nuclear pores, patch recording greatly underestimates their number. Assuming a pore has a conductance of 1,000 pS (90 Å diameter, 800 Å long[30], and containing a solution of 100 ohm . cm), then an upper limit for total nuclear conductance is 4 μS (0.25 megohm). If 80% of the pores have a conductance of 55 pS and 10%, of 200 pS (Fig. 3), then a lower limit for the total nuclear conductance is 0.25 μS (4 megohm). We measured 1 megohm or less, and our attempts to voltage-clamp with 70–90 megohm microelectrodes probably failed for this reason. If the pores are not the channels, either there are no pores in our patches, or the pores are closed. This explanation is surprising, because it is contrary to the view that nuclear pores are open holes. Even if the pores are artificially closed in our experiments, we must enquire about the function of the 200 pS channels in the natural state. We speculate that the role of these channels may be to balance the charge carried by macromolecules moving in and out of the nucleus, and therefore they could be involved in regulating gene expression and cell division. □

Received 6 October 1989; accepted 8 January 1990.

1. Bonner, W. M. *J. Cell Biol.* **64,** 421–430 (1975).
2. Bonner, W. M. *J. Cell Biol.* **64,** 431–437 (1975).
3. Feldherr, C. M. & Pomerantz, J. *J. Cell Biol.* **78,** 168–175 (1978).
4. De Robertis, E., Longthorne, R. F. & Gurdon, J. B. *Nature* **272,** 254–256 (1978).
5. Dabauvalle, M. C. & Franke, W. W. *Proc. natn. Acad. Sci U.S.A.* **79,** 5302–5306 (1982).
6. Feldherr, C. M., Cohen, R. J. & Ogburn, J. A. *J. Cell Biol.* **96,** 1486–1490 (1983).
7. Feldherr, C. M., Kallenbach, E. & Schultz, N. *J. Cell Biol.* **99,** 2216–2222 (1984).
8. Lanford, R. E. & Butel, J. S. *Cell* **37,** 801–813 (1984).
9. Lanford, R. E., Kanda, P. & Kennedy, R. C. *Cell* **46,** 575–582 (1986).
10. Newmeyer, D. D., Finlay, D. R. & Forbes, D. J. *J. Cell Biol.* **103,** 2091–2102 (1986).
11. Newmeyer, D. D., Lucocq, J. M., Burglin, T. R. & DeRobertis, E. D. *EMBO J.* **5,** 501–510 (1986).
12. Steven, B. J. & Swift, H. *J. Cell Biol.* **31,** 55–77 (1966).
13. Zasloff, M. *Proc. natn. Acad. Sci. U.S.A.* **80,** 6436–6440 (1983).
14. Dworetzky, S. I. & Feldherr, C. M. *J. Cell Biol.* **106,** 575–584 (1988).
15. Feldherr, C. M. *J. Cell Biol.* **20,** 188–192 (1964).
16. Horowitz, S. B. & Moore, L. C. *J. Cell Biol.* **6,** 405–415 (1974).
17. Frank, M. & Horowitz, S. B. *J. Cell Sci.* **19,** 127–139 (1975).
18. Paine, P. L., Moore, L. C. & Horowitz, S. B. *Nature* **254,** 109–114 (1975).
19. Horowitz, S. B. *J. Cell Biol.* **54,** 609–625 (1972).
20. Century, T. J., Fenichel, I. R. & Horowitz, S. B. *J. Cell Sci.* **7,** 5–13 (1970).
21. Century, T. J. & Horowitz, S. B. *J. Cell Sci.* **16,** 465–471 (1974).
22. Dingwall, C. & Laskey, R. A. *A. Rev. Cell Biol.* **2,** 367–390 (1986).
23. Newport, J. W. & Forbes, D. J. *A. Rev. Biochem.* **56,** 535–565 (1987).
24. Gerace, L. & Burke, B. *A. Rev. Cell. Biol.* **4,** 335–374 (1988).
25. McGrath, J. & Solter, D. *Science* **220,** 1300–1302 (1983).
26. Loewenstein, W. R. & Kanno, Y. *J. gen. Physiol.* **46,** 1123–1140 (1963).
27. Kanno, Y. & Loewenstein, W. R. *Expl Cell Res.* **31,** 149–166 (1963).
28. Coronado, R., Rosenberg, R. L. & Miller, C. *J. gen. Physiol.* **76,** 425–446 (1980).
29. Coronado, R. & Miller, C. *J. gen. Physiol.* **79,** 529–547 (1982).
30. Unwin, P. N. T. & Milligan, R. A. *J. Cell Biol.* **93,** 63–75 (1982).

ACKNOWLEDGEMENTS. We thank Elizabeth F. Smith for doing the electron microscopy, and David Clapham, Winfield Sale and Larry Rizzolo for a critical reading of the manuscript.

A serine protease triad forms the catalytic centre of a triacylglycerol lipase

Leo Brady, Andrzej M. Brzozowski*, Zygmunt S. Derewenda†, Eleanor Dodson, Guy Dodson, Shirley Tolley, Johan P. Turkenburg, Lars Christiansen‡, Birgitte Huge-Jensen‡, Leif Norskov‡, Lars Thim‡ & Ulrich Menge§

Department of Chemistry, University of York, Heslington, York YO1 5DD, UK
‡ Novo-Nordisk A/S, Novo Alle, DK-2880 Bagsvaerd, Copenhagen, Denmark
§ Department of Enzyme Technology, GBF, D-3300 Braunschweig, FRG

TRUE lipases attack triacylglycerols and act at an oil–water interface; they constitute a ubiquitous group of enzymes catalysing a wide variety of reactions, many with industrial potential. But so far the three-dimensional structure has not been reported for any lipase. Here we report the X-ray structure of the *Mucor miehei* triglyceride lipase and describe the atomic model obtained at 3.1 Å resolution and refined to 1.9 Å resolution. It reveals a Ser . . His . . Asp trypsin-like catalytic triad with an active serine buried under a short helical fragment of a long surface loop.

M. miehei triacylglycerol lipase is a single polypeptide chain protein made up of 269 residues (molecular weight of an unmodified chain is 29,472). Isolation and purification methods have already been described[1,2]. The gene encoding the complete enzyme precursor has been sequenced[2]. A recombinant plasmid was introduced and expressed in *Aspergillus oryzae*[3]. The purified protein was dissolved in 20 mM Tris-HCl buffer, pH 8.05, to a concentration of 15–16 mg ml^{-1}; we used the hanging drop technique with high concentrations of phosphate buffer (55–75% v/v of saturated solution) to obtain single crystals suitable for X-ray structural study. The crystals have the symmetry of space group $P2_12_12_1$, with the unit cell having dimensions $a = 71.6$ Å, $b = 75.0$ Å and $c = 55.0$ Å. If we assume one molecule per asymmetric unit, the specific volume[4] is 2.5 $Å^3$ per dalton.

Table 1 summarizes the crystallographic results. A single major site in the Hg derivative was used to obtain the initial single isomorphous replacement anomalous scattering phases, which allowed the identification of three Pt sites using difference Fourier techniques. The resulting set of phases obtained with two derivatives (mean figure of merit, $\langle m \rangle = 0.58$) was used to identify five principal sites in the iodinated derivative. Subsequent difference Fourier calculations using all three derivatives revealed two other secondary Hg sites and four more iodine sites. Recalculation of phases gave $\langle m \rangle = 0.74$. The initial electron density map calculated at 3.2 Å resolution using only two derivatives (Hg and Pt) was interpretable, although some features of the structure were obscure. A partial model consisting of ~70% of the molecule was constructed and used for a phase combination procedure. At the same time, a third derivative (I) was included in the isomorphous phasing, which led to a substantial improvement in the quality of the multiple isomorphous

* Permanent address: Department of Crystallography, Institute of Chemistry, University of Lodz, 91416 Lodz, Poland.
† To whom correspondence should be addressed.